Protein Expression and Purification 186 (2021) 105929

Contents lists available at ScienceDirect

Protein Expression and Purification

journal homepage: www.elsevier.com/locate/yprep

Recombinant organophosphorus hydrolase (OPH) expression in *E. coli* for the effective detection of organophosphate pesticides

Monika Jain, Priyanka Yadav, Bhavana Joshi, Abhijeet Joshi **, Prashant Kodgire *

Discipline of Biosciences and Biomedical Engineering, Indian Institute of Technology, Indore, Simrol, Khandwa Road, Indore, 453552, India

ARTICLE INFO

Keywords:
Colorimetric sensor
Encapsulated enzyme
Fluorometric detection
Organophosphates (OPs)
Organophosphorus hydrolase (OPH)

ABSTRACT

Accumulation and exposure of organophosphate pesticides are of great concern today owing to their abundant usage and potential health hazards. Harmful effects of organophosphate pesticide exposure and limitations of the available treatment methods necessitate the development of reliable, selective, cost-effective, and sensitive methods of detection. We developed a novel biosensor based on the enzymatic action of recombinant organophosphorus hydrolase (OPH) expressed in *E. coli*. We report the development of colorimetric biosensors made of His-Nus-OPH as well as His-Nus-OPH loaded alginate microspheres. The colorimetric detection method developed using solution-phase and alginate-encapsulated His-Nus-OPH exhibited detection limits of 0.045 and 0.039 mM, respectively, for ethyl paraoxon, and 0.101 and 0.049 mM, respectively, for methyl parathion. Additionally, fluorescence measurement using pH-sensitive fluorescein isothiocyanate (FITC) was used to sense the quantity of organophosphorus pesticides. The fluorometric detection method using solution-phase His-Nus-OPH, with ethyl paraoxon and methyl parathion as the substrate, reveals the lower limit of detection as 0.014 mM and 0.044 mM, respectively. Our results demonstrate the viability of His-Nus-OPH for OP detection with good sensitivity, LOD, and linear range. We report the first use of *N*-terminal His-NusA-tagged OPH, which enhances solubility significantly and presents a significant advance for the scientific community.

1. Introduction

In modern times, pesticides have gained prominence in a variety of sectors, from agriculture to industry, due to the needs and expectations of a growing population. The global usage of pesticides is to the tune of 3 million tons annually [1]. Of the known pesticides, four classes are most prominent: organophosphates (OPs), organochlorines, pyrethroids, and carbamates [2,3]. Among these, OPs are very popular, especially in developing countries, due to cost-efficient synthesis and ubiquitous and proven use as pesticides/insecticides. The prevalence of organophosphate pesticides is as high as 33% in developed countries and 50–60% in developing nations, where they pose a greater risk [4–6]. From a clinical point of view, there are some major concerns related to OPs, like blockage of the active site of acetylcholinesterase (AChE), which is the important enzyme of the nervous system required for the breakdown of acetylcholine. The build-up of acetylcholine resulting from inhibition of AChE results in neurological complications, and the problem extends to all vertebrates, including humans [7–9]. Clinically, in humans, OP poisoning cases are treated with anticholinergic drugs like atropine and/or acetylcholinesterase reactivators comprised of different types of oximes [10]. However, the efficacy of such treatment is inconclusive, with reports citing side effects and even increased morbidity [11,12]. Moreover, long term OP exposure results in an "aging effect" on neuropathy target esterase (loss of alkyl group bound to phosphorus), which progressively and irreversibly inhibits the esterase over time, leading to OP-induced neuropathy [13]. OP poisoning has a high rate of mortality, reported in various studies to be between 22% and 50%, which exceeds normal expectations [14–16] and is also reported to be similar irrespective of economic status or condition of the patients' country [17]. Combined with the relative ease of exposure, these compounds present a pertinent risk for healthcare professionals to mitigate effectively.

Due to the above concerns, the development of a reliable, selective, sensitive detection and detoxification method for these compounds is necessary. Some soil microbiota have been shown to have enzymes that can degrade these toxic compounds into non-toxic compounds [18]. Organophosphorus Hydrolase (OPH) enzyme isolated from *Flavobacterium* sp. and *Pseudomonas diminuta* has shown this activity of degradation of OPs. OPH has a broad substrate specificity, including the

* Corresponding author.
** Corresponding author.
E-mail addresses: abhijeet.joshi@iiti.ac.in (A. Joshi), pkodgire@iiti.ac.in (P. Kodgire).

https://doi.org/10.1016/j.pep.2021.105929
Received 13 December 2020; Received in revised form 18 May 2021; Accepted 7 June 2021
Available online 14 June 2021

cleavage of P–O, P–S, P–F, and P–CN bonds, it catalyzes the hydrolysis of organophosphorus compounds, such as methyl and ethyl parathion, paraoxon, chlorpyrifos, coumaphos, cyanophos, and diazinon as well as chemical warfare agents, such as sarin and soman [19]. Enzymatic hydrolysis is reportedly 40–2450 times faster compared to chemical hydrolysis [20] and thus attracts great interest from a scientific viewpoint for the remediation as well as detection of organophosphorus compounds in the environment.

The high-resolution X-ray structure showed that the OPH folds into αβ barrel motif called TIM Barrel [21]. OPH adopts TIM barrel fold where the active site is located at the C terminal of the β barrel [22]. The OPH active site is comprised of two Zn(II) ions enclosed inside a (β/α) 8-barrel motif, bridged by a carboxylated Lys-169 and a hydroxyl ion at neutral pH, with each Zn ion coordinated with various residues the α-Zn^{2+} being coordinated to His-55, His-57, Asp-301, the carboxylated Lys-169 and the hydroxide, while the β-Zn^{2+} is coordinated to His-201, His-230, carboxylated Lys-169, the hydroxide and an H_2O molecule [23]. The enzyme can catalytically hydrolyze phosphotriesters/organophosphates by a mechanism involving cleavage of the phosphotriester bond in an SN2-type reaction mechanism with the involvement of an H_2O molecule terminally bound to the α-metal ion, whose pKa is lowered due to the interaction with the metal ion and the bridging hydroxide, leading to the generation of a hydroxide nucleophile that is optimally aligned for an attack on the electrophilic phosphorus [24]. Fig. 1 shows a representative schematic of the hydrolysis of ethyl paraoxon and methyl parathion by OPH. The hydrolysis process in the presence of $CoCl_2$ [25] results in the production of *p*-nitrophenol along with the release of two protons, which form the basis of the colorimetric and fluorometric detection methods used in several studies. Detailed discussions on the reaction mechanism of OPH with OP compounds have been described in the literature [26,27].

In the literature, there are several reports on the sensing of

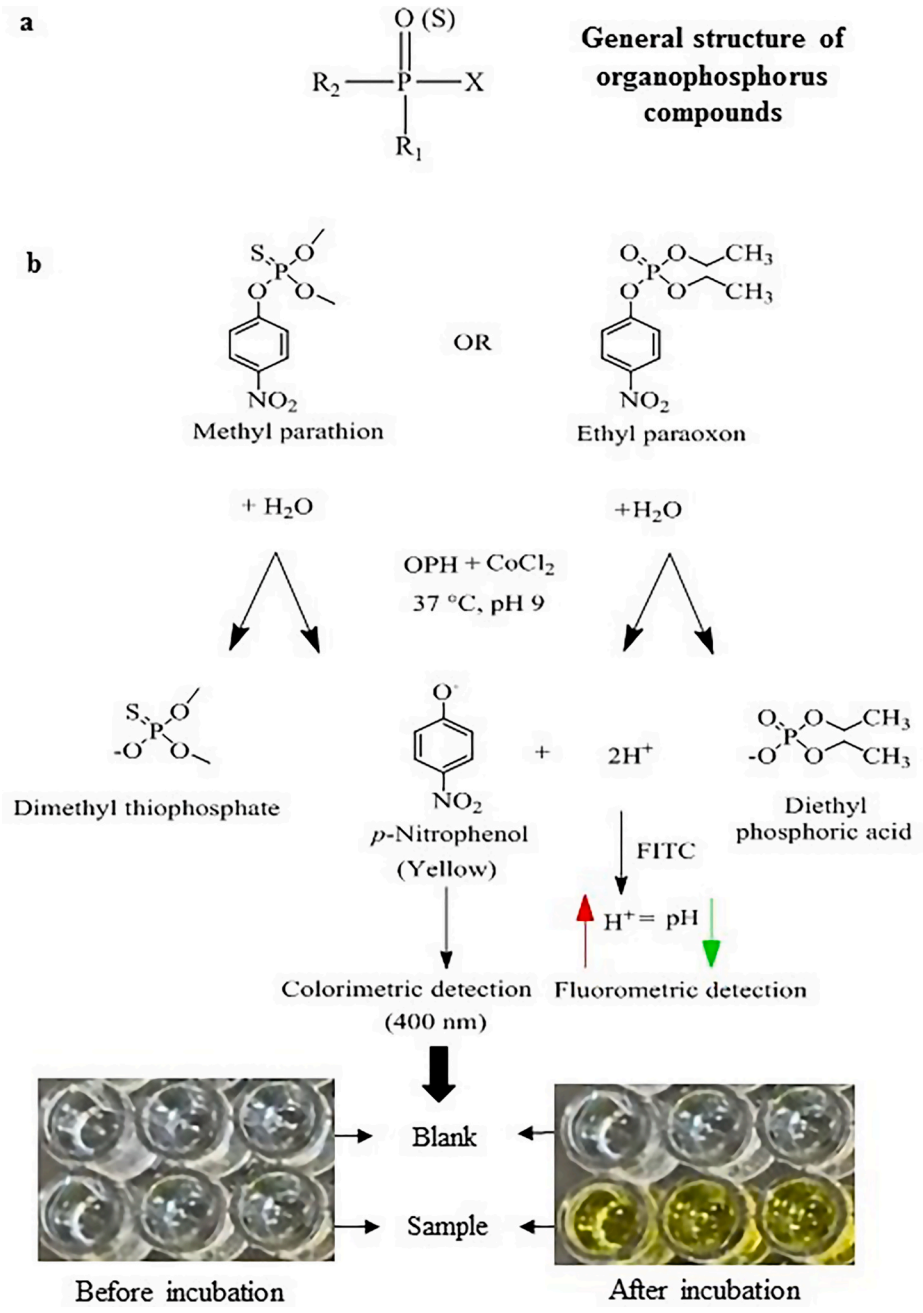

Fig. 1. OPH reaction mechanism. **(a)** The general structure of organophosphorus compounds. R1 and R2 are commonly represented by alkoxy groups, although other chemical substitutes are also possible (like phenyl for R1 and methoxy to butoxy for R2); the phosphorus is also attached to either an oxygen or sulphur atom via a double bond. X represents the "leaving group" displaced when acetylcholinesterase (AChE) is phosphorylated by the OP and thus is most sensitive to hydrolysis. X is either a phenoxy group or a fluorine. **(b)** Depiction of hydrolysis of OP compounds in presence of His-Nus-OPH with *p*-nitrophenol and H^+ as a product which can be detected by colorimetric and fluorometric detection methods, respectively.

organophosphorus compounds using OPH through electrochemical, optical, and other methods [28]. However, an optimal sensor that achieves good enzymatic catalytic activity and low enough detection limits to detect organophosphorus compounds in practical use cases remain elusive primarily due to reproducibility and cost concerns. In this article, we report colorimetric, as well as fluorescence-based sensing using a known fluorescent dye (FITC) of organophosphorus compounds by the interaction of His-Nus-OPH with OP compounds such as methyl parathion and ethyl paraoxon.

2. Materials and methods

2.1. Materials

Strains and chemicals: A *opd* gene construct was received from Prof. D. Siddavattam (Dept. of Animal Biology, School of Life Sciences, University of Hyderabad, Hyderabad-500046, India). In this study, we used the *oph* gene without signal peptide. The *E. coli* cells, DH5α and Rosetta, were used as host cells, and pET43a and pET28a vector (Novagen) were used for cloning and expression of OPH.

Favor Prep plasmid extraction mini kit was purchased from Favorgen (Taiwan), GeneJET gel extraction kit and GeneJET PCR purification kit were purchased from Thermo Scientific (USA), Agarose, Luria Bertani Broth Miller, Kanamycin, Sodium chloride, Imidazole, *Pfu* and *Taq* DNA polymerase, Lysozyme, Bradford reagent were purchased from HiMedia (India), *Spe*I, *Nde*I, *Xho*I, and T4 DNA Ligase were purchased from NEB (USA). dNTPs, Ethidium bromide, Tris-Cl, 2-(Cyclohexylamino) ethanesulfonic acid (CHES) buffer, Methyl parathion, Ethyl paraoxon, Sodium alginate, Fluorescein isothiocyanate (FITC) dextran 500 kDa were purchased from Sigma Aldrich (USA), Cobalt chloride was purchased from Loba Chemie (India), and Calcium chloride from Otto Chemie (India), were used for cloning, expression, purification and activity of recombinant OPH.

2.2. Cloning of OPH with N- terminal His tag

The *oph* gene was obtained from *Pseudomonas diminuta* (accession number P0A434.1). *oph* gene was cloned into the pET28 expression vector by using *Nde*I and *Xho*I site with *N*-terminal 6X His tag. The *oph* gene was amplified by using *Pfu* DNA polymerase and primers PK671F and PK673R (Table S1) (Sigma Aldrich, USA). Thermal cycles were programmed for 2 min as initial denaturation, and subsequently 30 cycles of 30 s for denaturation at 95 °C, 30 s at 59 °C as annealing temperature, 90 s at 72 °C for the extension, and a final extension at 72 °C for 10 min. The resultant PCR product for the *oph* gene is 1011 bps. Insert, and vector DNA were both double digested by *Nde*I and *Xho*I restriction enzymes. The insert and vector DNA were ligated, followed by the transformation of ligated samples into *E. coli* DH5α cells. The presence of insert DNA in the plasmid construct was confirmed by colony PCR, further, the recombinant plasmids were isolated from the replica plates and then sequenced by Sanger sequencing. The recombinant clones designated as p28-His-OPH were then transformed into *E. coli* Rosetta cells.

2.3. Sequential cloning of OPH in pET43 and pET28 with N- terminal His tag and NusA tag

Briefly, OPH was initially cloned into pET43 by using *Spe*I and *Xho*I site with the *N*-terminal NusA tag, with a preScission protease site in between the NusA tag and OPH to generate p43-Nus-OPH (8023 bps). Subsequently, the Nus-OPH fragment was released using *Nde*I and *Xho*I site and cloned into the pET28 expression vector to generate an *N*-terminal His-NusA tag. OPH was amplified by using *Pfu* DNA polymerase and primers PK672F and PK673R (Table S1) and cloned into plasmid pET43. Thermal cycles were programmed for 5 min as initial denaturation, and subsequently 30 cycles of 30 s for denaturation at 95 °C, 30 s at 59 °C as annealing temperature, 90 s at 72 °C for the extension, and a final extension at 72 °C for 10 min. The resultant PCR product of the *oph* gene is 1011 bps. Insert, and vector DNA were both double digested by using *Spe*I, *Xho*I restriction enzymes and cloned into pET43 vector. Later, the Nus-OPH fusion gene fragment was excised using *Nde*I and *Xho*I sites and cloned into a pET28 vector to generate p28-His-Nus-OPH (7819 bps). The presence of insert DNA in the plasmid construct was confirmed by colony PCR, the recombinant plasmids were isolated from the replica plates and then sequenced by Sanger sequencing. The recombinant clones were then transformed into *E. coli* Rosetta cells.

2.4. Expression of recombinant OPH

A single colony of *E. coli* Rosetta cells transformed OPH clone (p28-His-OPH or p28-His-Nus-OPH) was inoculated into a 5 ml LB tube with Kanamycin 10 μg/ml working concentration and was incubated at 37 °C and 200 RPM for 10–12 hours (h), followed by re-inoculation of 50 μl overnight grown culture into a fresh 5 ml LB tube with kanamycin and incubation at 37 °C and 200 RPM for 2–3 h until OD 600 reaches 0.8. This culture was then induced with 0.1 mM IPTG and 0.1 mM $CoCl_2$ and incubated at 180 RPM, with the conditions set at 37 °C/3 h and 16 °C/16 h for p28-His-OPH as well as p28-His-Nus-OPH. Subsequently, the cells were harvested at 8000 RPM at 4 °C for 10 min. The resultant pellet was washed and resuspended with 50 mM Tris-Cl, pH 7.4, with 10% glycerol. Afterwards, lysozyme was added to a final concentration of 100 μg/ml and then incubated at 30 °C for 20 min, followed by sonication and centrifugation of cell lysate at 14000 rpm and 4 °C for 10 min. The lysate was then analysed on 12% SDS PAGE for p28-His-OPH and p28-His-Nus-OPH.

2.5. Purification of recombinant His-Nus-OPH

All steps of affinity chromatography were performed at 4 °C using His-trap Ni-column (GE) with AKTA Unichromat 1500 (GE). After expression, the concentration of components in the input sample for purification was made equivalent to the equilibration buffer (50 mM Tris-Cl pH 8.0, 500 mM NaCl, and 10 mM imidazole). This input sample was loaded on the pre-equilibrated column at a flow rate of 1 ml/min. Subsequently, the column was washed with wash buffers comprising 50 mM Tris-Cl, pH 8.0, 500 mM NaCl, with 50 mM and 90 mM imidazole, respectively. The expression level of the 6X His tagged protein mainly determines the number of wash steps required for a high level of purification. The sample was then eluted using an elution buffer comprising 50 mM Tris-Cl, pH 8.0, 500 mM NaCl, with 300 mM imidazole. All fractions were analysed on an 8% SDS PAGE.

2.6. SDS-PAGE

The same volume of each sample was mixed with the sample buffer (0.25 M Tris-Cl, pH 6.8, 10% SDS, 0.05 M β-mercaptoethanol, 50% glycerol, 0.5% bromophenol blue), boiled for 5 min and analysed by either 8% or 12% SDS PAGE for His-Nus-OPH and His-OPH.

2.7. Activity assay of recombinant His-Nus-OPH

The method to perform the activity assay was adapted from the report by Meier et al. [29]. Concisely, 1 μl of protein was mixed with 50 mM CHES [2-(*N*-cyclohexyl amino) ethane-sulfonic acid] buffer, pH 9.0, 0.1 mM $CoCl_2$, 1 mM methyl parathion and/or ethyl paraoxon (Sigma), and the final volume was made up to 200 μl with SDW. The reaction mixtures were incubated at 37 °C for 5 min in the case of solution-phase His-Nus-OPH, 10 min for encapsulated His-Nus-OPH with ethyl paraoxon, and 20 min for encapsulated His-Nus-OPH with methyl parathion. The activity was calculated by measuring the absorbance of *p*-nitrophenol produced due to the hydrolysis of methyl parathion and/or ethyl paraoxon at 400 nm (ε400 = 17,000/M/cm for *p*-nitrophenol) [29] by

using a plate reader (SYNERGY H1 microplate reader). Specific activities were expressed as units (micromoles of methyl parathion and/or ethyl paraoxon hydrolyzed per minute) per milligram of total protein. Encapsulated protein enzymatic activity was also performed similarly by taking 330 μl encapsulated protein microspheres and making up to 500 μl.

The kinetic parameters of solution-phase and encapsulated His-Nus-OPH with ethyl paraoxon and methyl parathion were determined using substrate concentrations of 0.1–9 mM. kinetic parameters for ethyl paraoxon and methyl parathion substrate (k_{cat}, K_m, V_{max}, k_{cat}/K_m) were calculated following the method described in the previously published literature [30].

2.8. Effect of temperature and pH on the activity of recombinant His-Nus-OPH

To determine the optimal temperature for His-Nus-OPH with ethyl paraoxon, we tested its activity at varying temperatures ranging from 20 to 45 °C for 10 min, in 50 mM CHES buffer, pH 9.0, 0.1 mM $CoCl_2$, and 1 mM ethyl paraoxon.

In order to determine the optimal pH for His-Nus-OPH with ethyl paraoxon, we performed activity tests at a pH range of 6–10, at 37 °C for 10 min, in either 50 mM sodium phosphate buffer (pH 6.0, 6.5, 7.0, 7.5 and 8.0, respectively) or 50 mM CHES buffer (pH 8.5, 9.0, 9.5 and 10.0, respectively), 0.1 mM $CoCl_2$, and 1 mM ethyl paraoxon.

Enzymatic activity assays were performed in a similar manner as described in the above section.

2.9. Encapsulation of His-Nus-OPH and FITC-dextran/His-Nus-OPH in alginate microspheres using an ultrasonic atomizer

The method to perform encapsulation was adapted from the report by Pandey G. et al. [31]. His-Nus-OPH protein (0.2–0.65 mg/ml) was encapsulated in 0.7% sodium alginate microspheres formulated via ionic gelation technique by using 4% calcium chloride to form Calcium alginate microspheres. The protein alginate mixtures were sprayed using an ultrasonic atomizer (Sonozap, USA) at optimized instrumental parameters like frequency 130 kHz and 3.5 Watt of power with the flow rate of 0.3 ml/min using a syringe pump (Multi-phaserTM, model NE-300, New Era pump system, USA) and collected in 40 ml 4% w/v calcium chloride stirred on a magnetic stirrer at 1500 rpm. Particles prepared were separated using a refrigerated high-speed centrifuge (Kubota-7000, Japan) at 7000 g, after three washing cycles of 15 min with sterile distilled water. FITC dextran (1 mg) and His-Nus-OPH (0.5 mg) were encapsulated in alginate (0.7% w/v) microspheres formed by ionic gelation technique using an ultrasonic atomizer with optimized instrumental parameters as described above using 4% w/v calcium chloride as a crosslinker. FITC dextran (1 mg) was separately encapsulated in alginate (0.7% w/v) microspheres by the same technique to act as a control. Both dye loaded particles and co-immobilized particles prepared were separated using a refrigerated high-speed centrifuge (Kubota-7000) at 7000 g, after three washing cycles of 15 min with sterile distilled water.

2.10. Characterization of alginate microspheres

Morphological characterization was done by scanning electron microscopy (SEM) using a Zeiss Supra 55 (Germany) machine. A thin layer of microspheres was evenly spread onto the glass slide. The slide was kept on the desiccator for 3 h in which silica adsorbed all the moisture present in the sample. The sample was coated with copper metal (Q150R Rotary-pumped sputter coater/carbon coater) and observed at an operating voltage of 5 kV. Alginate encapsulated FITC-Dextran, and FITC-Dextran/His-Nus-OPH high-resolution images were taken at 60× magnification using a confocal laser scanning microscope (CLSM) (FluoView 1000, Olympus America Inc. USA). The fluorescence excitation and emission wavelengths were selected as 488 nm and 520 nm, respectively. Particle size distribution measurements were performed using ImageJ software [32]. To confirm the encapsulation of His-Nus-OPH, beads were boiled at 95 °C for 15 min and then loaded on the 8% SDS PAGE along with the input and the first wash. The encapsulation efficiency for His-Nus-OPH protein in the alginate microspheres was determined in this study by calculating band intensities of encapsulated protein with reference to the input sample on an SDS PAGE. Intensities of protein bands were quantified using ImageJ software.

2.11. Biosensing studies of ethyl paraoxon and methyl parathion

Colorimetric biosensing of ethyl paraoxon and methyl parathion in solution-phase was performed by mixing His-Nus-OPH fusion protein with CHES buffer, pH 9.0, 0.1 mM $CoCl_2$ and incubating at 37 °C for 5 min. On the other hand, for encapsulated protein, enzymatic activity was also performed in a similar manner that is, incubating at 10 min for His-Nus-OPH encapsulated alginate microspheres with ethyl paraoxon and 20 min for methyl parathion. The OPH enzyme activity was calculated by exposing different concentrations of ethyl paraoxon and methyl parathion (0.005–1 mM) and measuring the increase in the absorbance of *p*-nitrophenol formed at 400 nm using an extinction coefficient 17,000 M/cm for *p*-nitrophenol. The method to perform fluorescence biosensing was adapted from the report by Zourob et al. and Doong et al. [33,34]. Fluorometric biosensing assay comprised of His-Nus-OPH fusion protein and FITC-dextran (1 mg/ml), which were mixed in ratio 1:12 (w/w) in the solution phase. Subsequently, 0.1 mM $CoCl_2$, ethyl paraoxon (0.001–0.5 mM) and methyl parathion (0.005–0.5 mM) was added to the mixture and the volume was made up to 1 ml. The reaction mixture was incubated for 5 min at 37 °C, and the decrease in the fluorescence intensity was recorded at 488 nm excitation and 519 nm emission by using a fluorometer (Horiba Fluoromax 4, Japan). Fluorescence changes in response to the catalytic activity of His-Nus-OPH in solution-phase were observed to evaluate the performance of His-Nus-OPH for the detection of OP compounds [35]. Fluorescence emission intensity ratios were plotted with respect to different concentrations of ethyl paraoxon and methyl parathion, and a linear regression analysis was performed to determine the calibration curves for estimation.

3. Results

3.1. Cloning and expression of OPH with N-terminal His tag in pET vector

The *oph* gene from *Pseudomonas diminuta* was cloned into pET28 expression vector, giving p28-His-OPH (Fig. 2a). The results of the expression of His-OPH in both pellet and supernatant are shown in Fig. 2b and c. From Fig. 2b at 37 °C for 3 h and Fig. 2c at 16 °C for 16 h induction, we observed no expression of His-OPH protein in the uninduced supernatant and pellet, but, incidentally, we found that on induction, the His-OPH protein was expressed in the pellet but not in the supernatant. Most likely, improper folding resulted in the formation of inclusion bodies [36], and hence more than 90% of the expression of His-OPH protein was observed in the pellet (Fig. 2b and c, lane 4 and 5, respectively).

3.2. Cloning, expression, and purification of OPH with N-terminal His and NusA tag in pET vector

Several recombinant proteins demonstrate poor solubility when overexpressed in a heterologous host [37]. To overcome the problem of solubility, the NusA solubilization tag was used. To obtain soluble OPH by bringing the *N*-terminal NusA tag, the *oph* gene was sequentially cloned into pET43 and pET28 expression vectors to give p43-Nus-OPH and p28-His-Nus-OPH, respectively. In pET43, the *oph* gene was cloned in such a way that a preScission protease site is present in

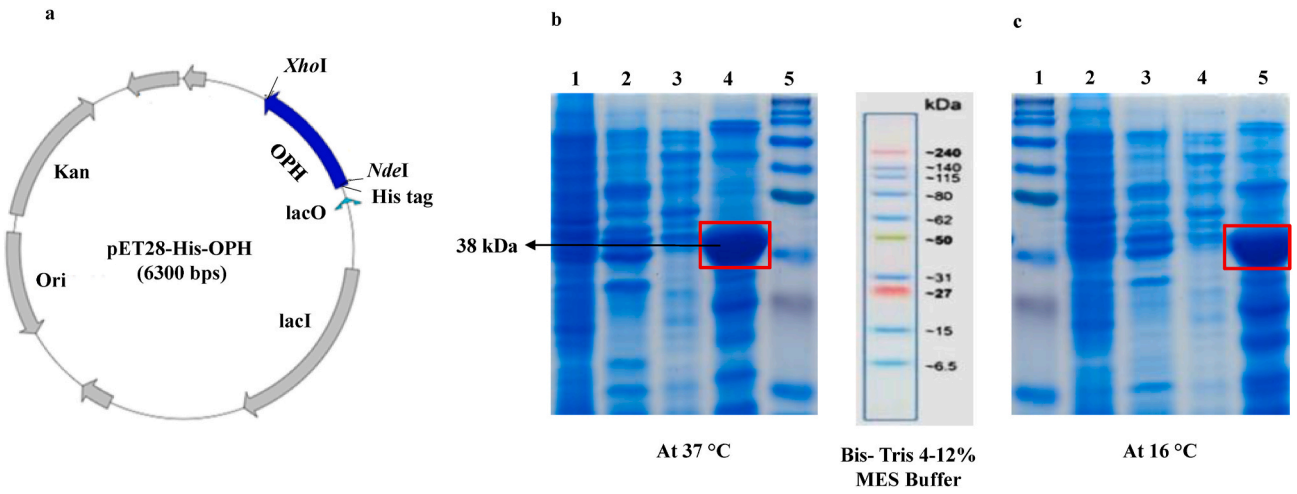

Fig. 2. Cloning and expression of OPH (p28-His-OPH) with *N*-terminal His tag in pET vector. **(a)** Map of pET28a with OPH, *N*-His tag. **(b)** Induction of recombinant His-OPH fusion protein. Induction of His-OPH was performed with 0.1 mM IPTG at 37 °C for 3 h. Lane 1: Uninduced supernatant, lane 2: uninduced pellet, lane 3: induced supernatant, lane 4: induced pellet, lane 5: protein marker. **(c)** Induction of His-OPH was performed at 16 °C for 16 h. Lane 1: Protein marker, lane 2: uninduced supernatant, lane 3: uninduced pellet, lane 4: induced supernatant, lane 5: induced pellet.

between the NusA tag and the OPH protein. The expression of these proteins, along with the solubilization tag, helps in getting expression in the soluble fraction [38]. To explore the possibility that bringing His tag on the *N*-terminal will assist in the purification step [39], the *oph* gene along with the NusA tag was double digested from the p43-Nus-OPH clone and sequentially cloned into pET28a expression vector by using *Nde*I and *Xho*I sites (Fig. 3a). The recombinant cloned plasmid was transformed into *E. coli* Rosetta cells and induced with 0.1 mM IPTG. Cell lysates were prepared and separated as supernatant and pellet to evaluate the amount of protein present in the soluble form. From Fig. 3b at 37 °C for 3 h induction, we observed no expression of His-Nus-OPH protein in the uninduced supernatant and pellet, but surprisingly we found that on induction, the His-Nus-OPH protein was expressed in the pellet but not in the supernatant (Fig. 3b, lane 4 and 5).

To explore the possibility of getting soluble protein via induction at a lower temperature, we decided to induce the cells at 16 °C. From Fig. 3c at 16 °C for 16 h induction, we observed no expression of His-Nus-OPH protein in the uninduced supernatant and pellet, but we found that on induction, the His-Nus-OPH protein expression was higher in the supernatant than the pellet (Fig. 3c, lane 4 and 5).

We observed an induced band of 93 kDa for His-Nus-OPH fusion protein in the soluble fraction, suggesting that low-temperature expression of OPH along with solubilization Nus-tag assists in getting His-Nus-OPH expressed in the soluble fraction. Since His-Nus-OPH carries an *N*-terminal His-tag, affinity purification of the recombinant His-Nus-OPH fusion protein was performed on a Ni-NTA resin. *N*-terminal His-tagged protein was able to bind to the Ni-NTA resin, and His-Nus-OPH protein was eluted by using 300 mM imidazole elution buffer (Fig. 3d, lane 6 to 8). Moreover, we were able to purify more than 90% pure His-Nus-OPH fusion protein due to the proper folding of protein facilitated by the presence of the NusA tag [40]. The affinity chromatogram of His-Nus-OPH is shown in Fig. S1.

3.3. Activity assay of recombinant His-Nus-OPH

To know whether the recombinant protein is indeed enzymatically

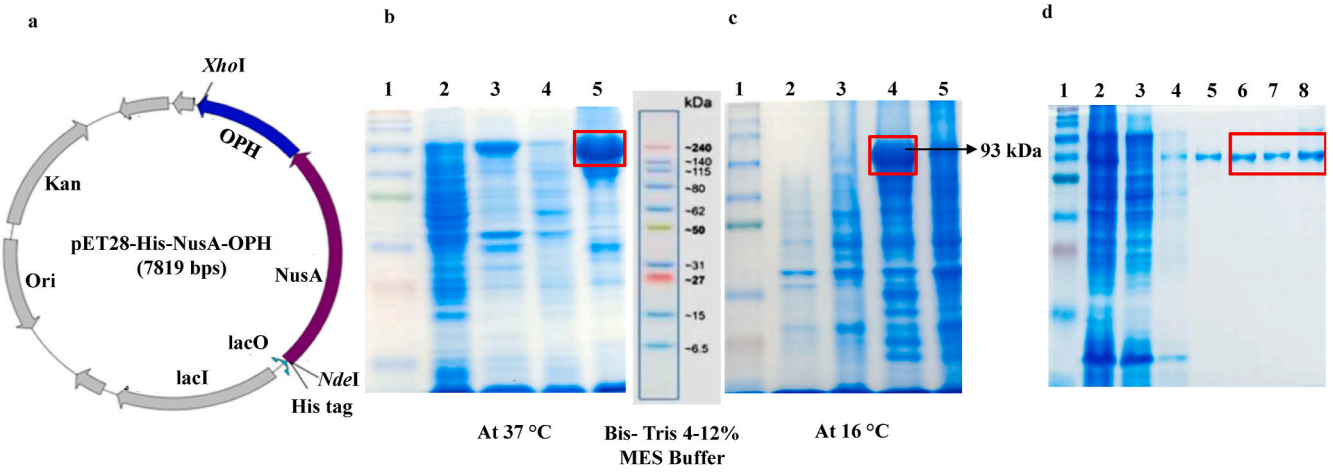

Fig. 3. Cloning, expression, and purification of OPH (p28-His-Nus-OPH) with *N*-terminal His and NusA tag in pET vector. **(a)** Map of pET28a with OPH, *N*-His-Nus tag. **(b)** Induction of recombinant His-Nus-OPH fusion protein. Induction was performed with 0.1 mM IPTG at 37 °C for 3 h. Lane 1: Protein marker, lane 2: uninduced supernatant, lane 3: uninduced pellet, lane 4: induced supernatant, lane 5: induced pellet **(c)** Induction of recombinant His-Nus-OPH fusion protein. Induction was performed at 16 °C for 16 h. Lane 1: Protein marker, lane 2: uninduced pellet, lane 3: uninduced supernatant, lane 4: induced supernatant, and lane 5: induced pellet. **(d)** Purification of recombinant His-Nus-OPH fusion protein. Lane 1: Protein marker, lane 2: induced cell extract, lane 3: flow-through, lane 4, 5: wash with 50, 90 mM Imidazole, lane 6 to 8: elution with 300 mM Imidazole.

active, we performed OPH enzyme assay. Recombinant His-Nus-OPH fusion protein demonstrated activity in the induced cell lysate as well as in purified fraction. Induced cell lysates were observed to be significantly more active than uninduced cell lysates for methyl parathion and ethyl paraoxon. However, purified samples showed higher specific activity as compared with the induced cell lysate. The specific activity of uninduced, induced, and purified His-Nus-OPH fusion protein was found to be 0.21 U/mg (±0.006), 24.12 U/mg (±1.22), and 333 U/mg (±45.11), respectively, for ethyl paraoxon and 0.57 U/mg (±0.003), 13.79 U/mg (±0.89), and 90.2 U/mg (±6.07), respectively, for methyl parathion (Fig. 4a and b) using a 1 mM concentration of the substrates. Thus, we observed that purified His-Nus-OPH has 13.8 and 6.5 times greater specific activity than the induced His-Nus-OPH with respect to ethyl paraoxon and methyl parathion, respectively, suggesting significant fold purification using affinity chromatography.

The kinetic parameters for ethyl paraoxon and methyl parathion as substrate using solution phase as well as encapsulated His-Nus-OPH have been reported in Table S2 and Figs. S2 and S3.

3.4. Effect of temperature and pH

Considering the significant specific activity with ethyl paraoxon, we studied the effect of temperature and pH on the activity of His-Nus-OPH in the solution phase. The effect of temperature on the activity of purified recombinant His-Nus-OPH was determined at varying temperatures ranging from 20 to 45 °C with an interval of 5 °C but also including 37 °C. In concurrence with earlier studies [41], His-Nus-OPH activity was found to gradually increase until 37 °C, and a subsequent rise in temperature decreased the activity. Hence, it is suggested that 37 °C is the optimum temperature for His-Nus-OPH with ethyl paraoxon (Fig. S4a).

The effect of pH on the activity of purified recombinant His-Nus-OPH was determined at a pH range of 6–10 with an interval of 0.5 pH units. These experiments showed the optimum activity at pH 9.0 for His-Nus-OPH (Fig. S4b).

3.5. Encapsulation of His-Nus-OPH and FITC-dextran/His-Nus-OPH in alginate microspheres using an ultrasonic atomizer

In recent times, encapsulation of proteins and cells are increasingly being explored in order to protect biomolecules from detrimental environmental factors such as pH changes, salts or reactive oxygen species, etc. [42]. To this end, materials such as polysaccharides and lipids have been used as encapsulants. Among these, alginate-based encapsulation has gained prominence due to its favourable properties such as good immobilization capacity, mechanical stability, water retention capability, heat stability, controllable porosity, low toxicity, and biocompatibility [43]. Proteins are encapsulated in different natural/synthetic polymers with an aim to maintain enzyme activity and increase stability. His-Nus-OPH protein was encapsulated in 0.7% sodium alginate by using an ultrasonic atomizer, chosen for reasons of high productivity, biocompatibility, mild gelation and formation conditions, industrial relevance, and good particle size distribution [44,45]. 4% $CaCl_2$ was used as a cross-linker to maximize bead formation and achieve a smaller particle size [46–48]. Ionic gelation is the main principle behind the formation of alginate microspheres from atomized droplets created using the ultrasonic atomizer due to ultrasonic waves. To optimize the particle size distribution of alginate microspheres, different instrumental parameters like frequency, flow rate, the distance of crosslinking were evaluated. Ultrasonic atomizer was utilized as described previously to co-immobilize FITC-dextran, which acts as a pH-sensitive fluorophore along with His-Nus-OPH.

3.6. Characterization of alginate microspheres

SEM analysis was performed to observe the encapsulation of His-Nus-OPH into the alginate microspheres revealing the spherical shaped porous microspheres of His-Nus-OPH ranging from 7 to 37 μm, and the average size of the particle was found to be 18.8 μm (Fig. 5 a-b). Moreover, the spherical morphology has been reported to enhance the stability and mechanical strength of the constituents [49]. Higher porosity of the alginate microsphere aids in the transport of analyte and product across the beads for continuous catalysis by the enzymes. The encapsulated FITC-Dextran and FITC-Dextran/His-Nus-OPH were characterized by confocal laser scanning microscopy (CLSM), which confirmed the successful incorporation of FITC-Dextran/His-Nus-OPH in the alginate microspheres (Fig. 5c and d). The CLSM analysis revealed that FITC-Dextran and FITC-Dextran/Nus-OPH microcarriers have typical particle sizes ranging from 3 to 22 μm and 10.7–30.4 μm, respectively, and average particle sizes of 13.0 μm and 20.5 μm, respectively.

Encapsulation efficiency is the percentage of protein that is successfully entrapped into the microspheres, which was determined in this study (Fig. 5e, lane 3 and 4 to 6). Subsequently, we estimated the encapsulation efficiency of His-Nus-OPH into the alginate microspheres by boiling the alginate microspheres and running these on 8% SDS-PAGE, along with input and wash controls (Fig. 5e). In general, we observed 10–20% encapsulation efficiency, and this value was used to calculate the amount of protein present inside alginate microspheres after encapsulation.

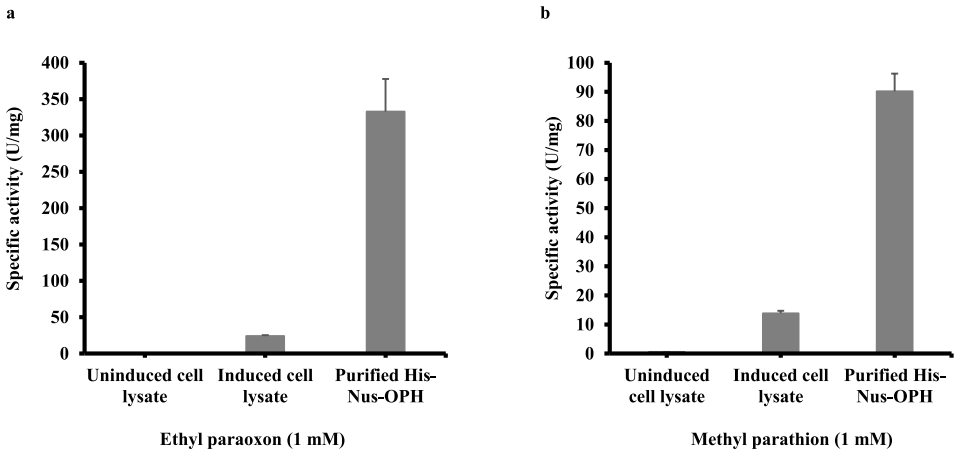

Fig. 4. Colorimetric activity assay of solution-phase His-Nus-OPH with different substrates. His-Nus-OPH with 1 mM substrate in the presence of CHES buffer, pH 9.0, at 37 °C for 5 min **(a)** 1 mM of ethyl paraoxon **(b)** 1 mM of methyl parathion. The values are represented as the average of duplicate samples, and the standard deviation is indicated by error bars. A representative result is shown based on at least three separate experiments.

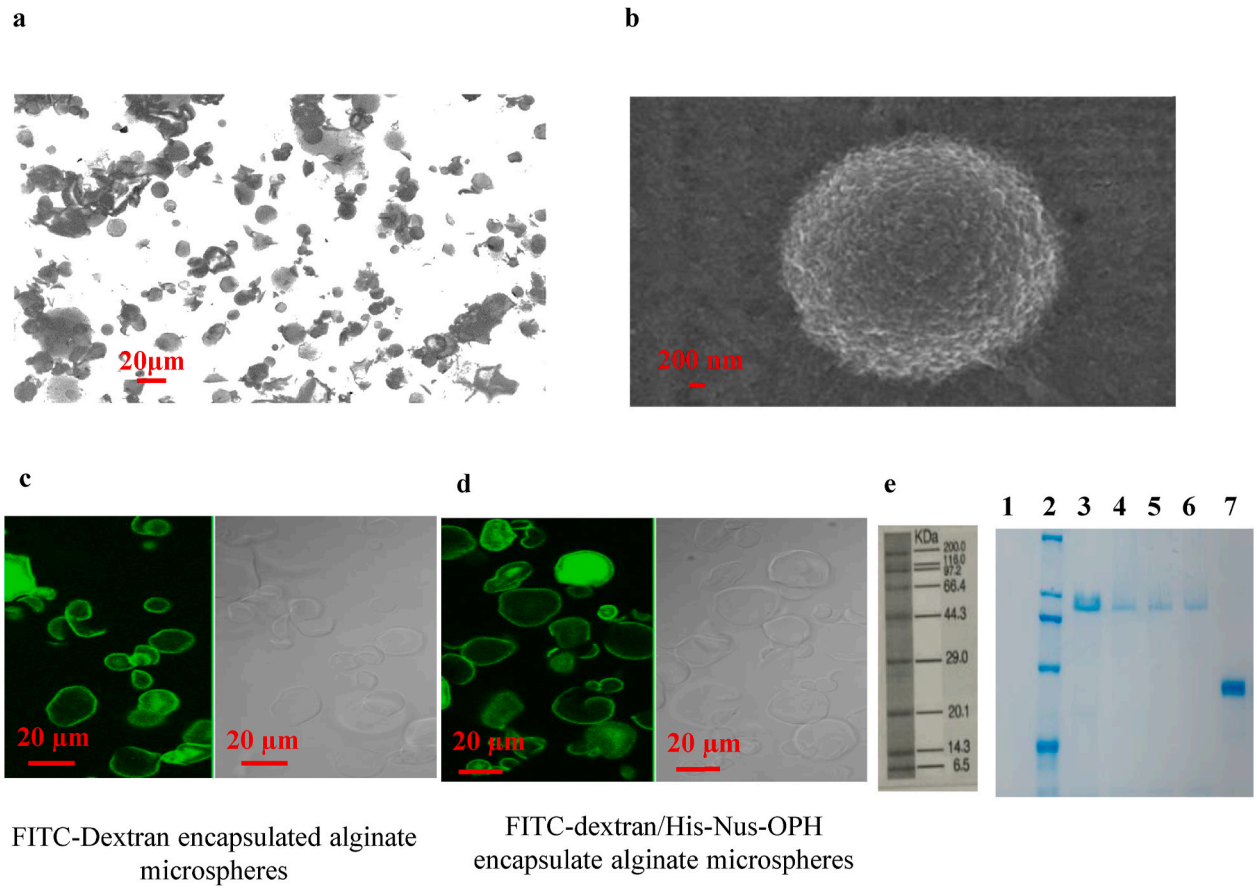

Fig. 5. Encapsulation and Characterization of His-Nus-OPH and FITC-dextran/His-Nus-OPH. SEM images of His-Nus-OPH loaded alginate microspheres with 0.7% alginate. Spherical shaped beads were observed in SEM. **(a–b)** His-Nus-OPH loaded alginate microspheres at 513 X and 55 K X magnification, respectively. **(c)** CLSM image of FITC-Dextran loaded alginate microcarriers at 60 X. **(d)** CLSM image of FITC-Dextran/His-Nus-OPH loaded alginate microcarriers at 60 X. At least three independent experiments were performed, and a representative result is shown. **(e)** Analysis of His-Nus-OPH loaded alginate microspheres using SDS PAGE. Lane 1: Unencapsulated His-Nus-OPH in wash 1 after buffer exchange, lane 2: protein marker, lane 3: input sample, lane 4 to 6: encapsulated His-Nus-OPH, lane 7: 2 µg of BSA.

3.7. Colorimetric biosensing of ethyl paraoxon and methyl parathion

Colorimetric biosensing of His-Nus-OPH was performed with 0.005, 0.025, 0.05, 0.5 and 1 mM of ethyl paraoxon and methyl parathion, respectively, and specific activity with respect to the aforementioned concentrations was found to be 0.72, 4.02, 7.47, 85.06, 155.25 U/mg with ethyl paraoxon and 0.56, 2.01, 6.13, 18.50, 35.05 U/mg for methyl parathion (Fig. 6a and b). Colorimetric biosensing of encapsulated His-Nus-OPH was performed with 0.1, 0.25, 0.5 0.6, 0.75, 0.8, 1 mM of ethyl paraoxon and 0.005, 0.01, 0.025, 0.05, 0.2, 0.3, 0.6, 0.8, 1 mM methyl parathion, respectively, and specific activity with respect to the after mentioned concentrations was found to be 1.07, 2.25, 4.15, 5.19, 6.32, 6.9 and 8.3 U/mg with ethyl paraoxon (Fig. 7a), and 0.07, 0.12, 0.34, 0.72, 1.67, 2.97, 4.77, 6.37 and 8.66 U/mg for methyl parathion (Fig. 7b).

The detailed parameters such as linear range, sensitivity, LOD, and

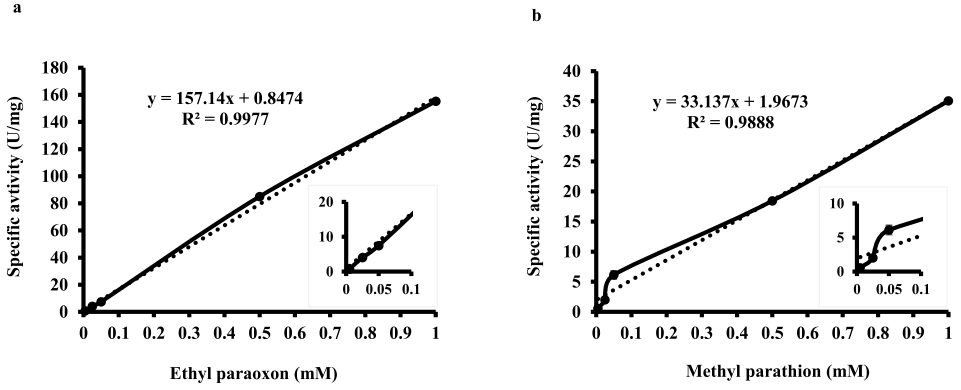

Fig. 6. Colorimetric activity assay of solution-phase His-Nus-OPH with different substrate concentrations. His-Nus-OPH with 0.005, 0.025, 0.05, 0.5, and 1 mM of the substrate in the presence of CHES buffer pH 9.0, at 37 °C for 5 min. **(a)** With ethyl paraoxon **(b)** With methyl parathion. The values are represented as the average of duplicate samples, and the standard deviation is indicated by error bars. A representative result is shown based on at least three separate experiments.

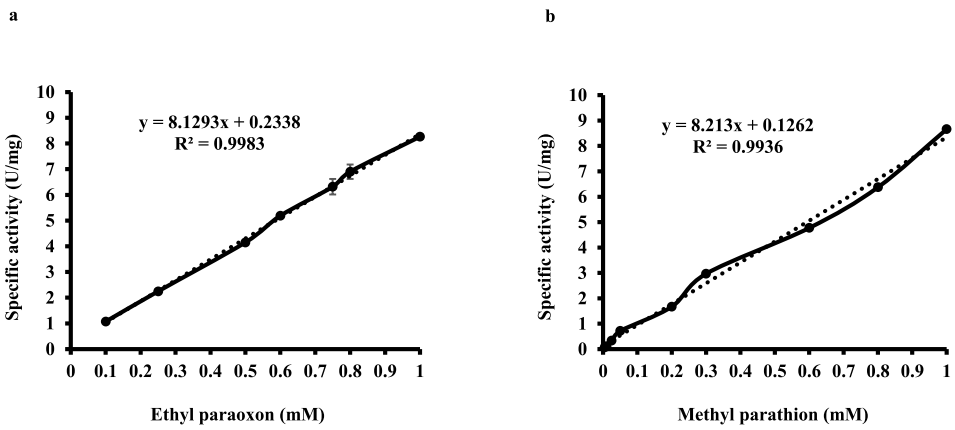

Fig. 7. Colorimetric activity assay of encapsulated His-Nus-OPH with different substrate concentrations. **(a)** Activity assay of His-Nus-OPH with 0.1, 0.25, 0.5, 0.6, 0.75, 0.8 and 1 mM of ethyl paraoxon, CHES buffer at 37 °C for 10 min. **(b)** Activity assay of His-Nus-OPH with 0.005, 0.01, 0.025, 0.05, 0.2, 0.3, 0.6, 0.8 and 1 mM of methyl parathion, CHES buffer at 37 °C for 20 min. The values are represented as the average of duplicate samples, and the standard deviation is indicated by error bars. A representative result is shown based on at least three separate experiments.

linearity of the solution-phase, as well as encapsulated His-Nus-OPH used in the colorimetric assay for ethyl paraoxon and methyl parathion, are given in Table 1A. The linear range for the detection of ethyl paraoxon was found to be 0.005–1 and 0.1–1 mM in the solution-phase and encapsulated phase, respectively. The change in the linear range for encapsulated His-Nus-OPH can be attributed to the diffusion barrier for both analyte and product in the catalytic reaction. Similarly, for methyl parathion linear range was 0.005–1 mM in the case of purified His-Nus-OPH enzyme in both solution-phase and encapsulated forms. In general, better detection limits are observed for encapsulated His-Nus-OPH compared to solution-phase His-Nus-OPH, that is, 0.039 and 0.049 mM for encapsulated His-Nus-OPH compared to 0.045 and 0.101 mM for solution-phase His-Nus-OPH, w.r.t. ethyl paraoxon and methyl parathion, respectively. It is observed that the assay with solution-phase and encapsulated His-Nus-OPH is more sensitive with greater linearity and lower LOD for ethyl paraoxon compared to methyl parathion. This difference between ethyl paraoxon and methyl parathion substrates is most likely due to the unfavourable interaction of methyl parathion in comparison to ethyl paraoxon with the enzymatic active site involved in the catalytic degradation of OPs. A previous report has indicated that the binding pocket of the OPH enzyme may preferably bind to larger substrates having ethoxy groups, such as ethyl paraoxon, compared to smaller substrates like methyl parathion [50]. The response time for the purified enzyme was found to be about 5 min, for both paraoxon and methyl parathion, in the solution phase. For the encapsulated enzyme, however, the response time for ethyl paraoxon and methyl parathion, respectively, was 10 min and 20 min. The increase in response time in the encapsulated phase is likely due to the additional diffusion barrier of alginate microspheres for interaction with the substrates.

3.8. Fluorescence biosensing of ethyl paraoxon and methyl parathion

The assay was developed based on a decrease in fluorescence intensity of pH-sensitive fluorophore FITC-dextran [51]. Upon the interaction of OPH with OP compounds, a decrease in pH of the solution occurs due to the release of protons with the concurrent release of *p*-nitrophenol [52]. The resultant drop in pH causes protonation of negatively charged FITC results in quenching of fluorescence, and this phenomenon was exploited to detect the presence of OPs (Fig. 8) [53]. To know optimum buffer and reaction conditions for fluorometric detection of OPs using His-Nus-OPH in solution-phase, we initially tested for a decrease in the fluorescence values (if any) of FITC in the different buffer concentrations. The reaction mixture was prepared with 0.1 mM $CoCl_2$, 1 mM ethyl paraoxon, His-Nus-OPH, FITC-dextran, and sterile distilled water up to 1 ml. We used 0 mM, 10 mM, and 50 mM activity buffer (CHES), respectively, and measured loss in the fluorescence values. It was observed that the reaction mixture with 0 mM CHES buffer showed a greater decrease in the intensity in comparison to the reaction mixture with the 10 and 50 mM concentration of CHES buffer in it. This could be because the presence of buffer neutralized the H^+ ions released during the reaction due to the inherent buffering capacity of the buffers. It is observed that the interaction of His-Nus-OPH with OP compounds such as ethyl paraoxon result in a decrease in fluorescence intensity of FITC dye over a time period of 0–20 min due to the progressive release of H^+ ions by the hydrolysis of OP compounds (Fig. 9 a, b). Thus, for all fluorescent sensing experiments, no CHES buffer was used. Moreover, when His-Nus-OPH:FITC (1:12) was used in solution-phase with 0.001, 0.005, 0.025, 0.05, 0.1, 0.3, 0.5 mM of ethyl paraoxon and 0.005, 0.025, 0.05, 0.1, 0.5 mM of methyl parathion, respectively, the rate of fluorescence decay increased with the concentration of substrate (Fig. 10 a, b). The 1:12 ratio of His-Nus-OPH: FITC was selected to optimize for good sensitivity [54].

Fluorescence-based bio-sensing of His-Nus-OPH with different concentrations of ethyl paraoxon and methyl parathion showed a linear range of 0.001–0.5 mM and 0.005–0.5 mM, respectively. The LOD of bio-sensing was 0.014 mM for ethyl paraoxon and 0.044 mM for methyl parathion, and the sensitivity defined as the slope of the linear concentration curve [55] was 95.96%/mM for ethyl paraoxon and

Table 1
Biosensing parameters of His-Nus-OPH.

Table 1 A Colorimetric biosensing parameters of solution-phase and encapsulated His-Nus-OPH

S. No.	Sample	Substrate	LOD (mM)	Sensitivity (U/mg/mM)	Linear range (mM)	Response time (Minutes)	Linearity (R^2)
1	Solution-phase His- Nus-OPH	Ethyl paraoxon	0.045	155.3	0.005–1	5	0.9977
		Methyl parathion	0.101	34.6	0.005–1	5	0.9888
2	Encapsulated His-Nus-OPH	Ethyl paraoxon	0.039	7.9	0.1–1	10	0.9983
		Methyl parathion	0.049	8.6	0.005–1	20	0.9936

Table 1 **B Fluorometric biosensing parameters of solution-phase His-Nus-OPH**

S. No.	**Sample**	**Substrate**	**LOD (mM)**	**Sensitivity (%/mM)**	**Linear range (mM)**	**Response time (Minutes)**	**Linearity (R^2)**
1	Solution-phase His-Nus-OPH	Ethyl paraoxon	0.014	95.96	0.001–0.5	5	0.9982
		Methyl parathion	0.044	47.2	0.005–0.5	5	0.9898

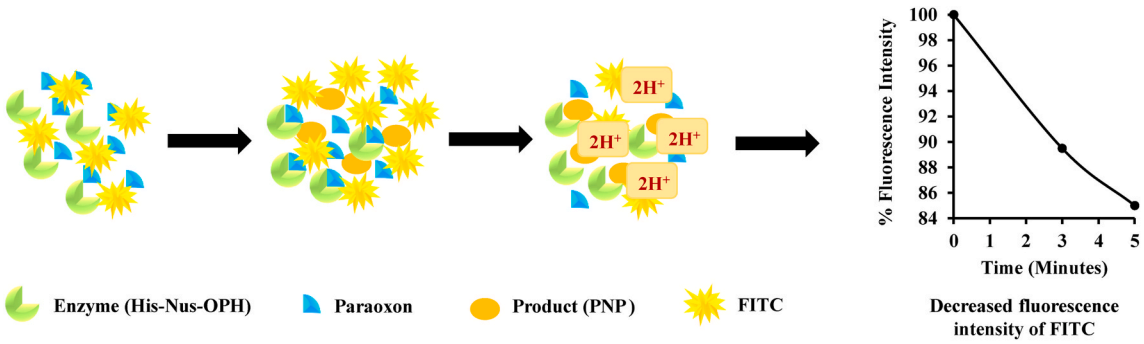

Fig. 8. Fluorescence assay mechanism of OPH using FITC dextran for detection of organophosphorus compounds.

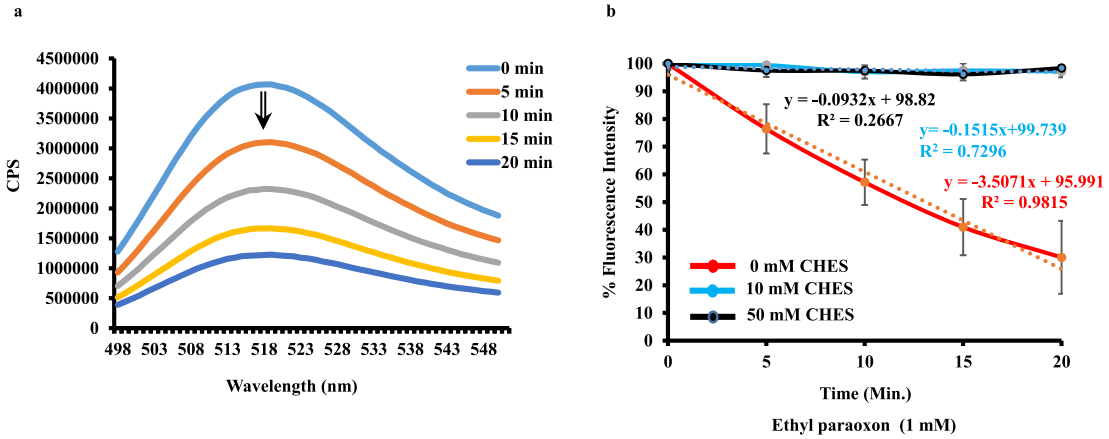

Fig. 9. Optimization of the concentration of CHES buffer for solution-phase His-Nus-OPH fluorescence assay. Fluorescence activity assay of solution-phase His-Nus-OPH enzyme detected using FITC, a pH-sensitive dye. With an increase in enzymatic activity, there is a decrease in pH which eventually results in a decrease in fluorescence intensity of FITC. **(a)** 0 mM CHES buffer was used at 37 °C, for 20 min with an interval of 5 min with ethyl paraoxon, and with an increase in time, fluorescence intensity was decreased. **(b)** 0 mM, 10 mM, and 50 mM CHES buffer were used at 37 °C, pH 9.0 for 20 min with an interval of 5 min with ethyl paraoxon. The decrease in the intensity of FITC was more in the case of the reaction mixture in which a 0 mM CHES buffer was used. The values are represented as the average of duplicate samples, and the standard deviation is indicated by error bars. A representative result is shown based on at least three separate experiments.

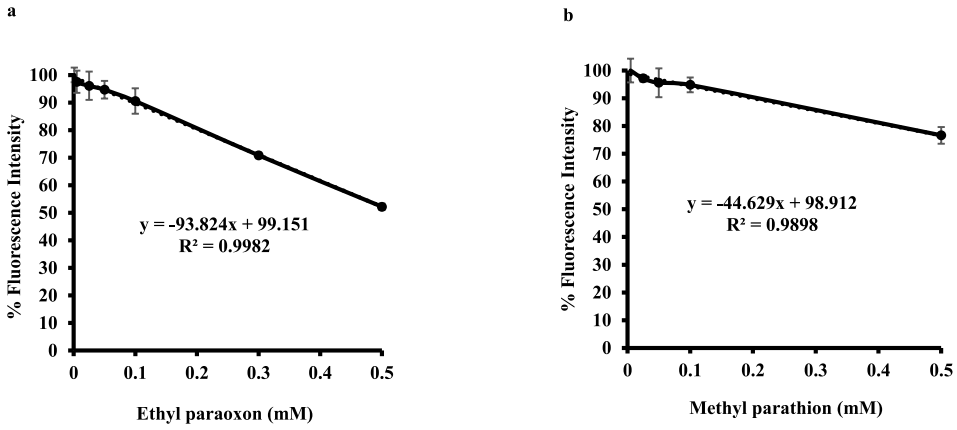

Fig. 10. Bio-sensing of ethyl paraoxon using solution-phase His-Nus-OPH via fluorescence assay. The 1:12 ratio of His-Nus-OPH and FITC-dextran was used at 37 °C, without activity buffer. **(a)** Fluorescence assay of His-Nus-OPH with 0.001, 0.005, 0.025, 0.05, 0.1, 0.3 mM, 0.5 mM of ethyl paraoxon, for 5 min. **(b)** Fluorescence assay of His-Nus-OPH with 0.005, 0.025, 0.05, 0.1, 0.5 mM of methyl parathion, for 5 min. The values are represented as the average of duplicate samples, and the standard deviation is indicated by error bars. A representative result is shown based on at least three separate experiments.

47.18%/mM for methyl parathion, respectively. The fluorescence intensity of FITC decreased linearly with an increase in the concentration of ethyl paraoxon or methyl parathion. Due to the increase in enzymatic activity, there is a decrease in pH, which eventually results in a decrease in the fluorescence intensity of FITC. The detailed parameters such as linear range, sensitivity, LOD, and linearity of the solution-phase His--Nus-OPH used in fluorescence assay with ethyl paraoxon and methyl parathion are given in Table 1B. It is observed that the assay with His-Nus-OPH is more sensitive with greater linearity and lower LOD for ethyl paraoxon compared to methyl parathion. Incidentally, the encapsulated His-Nus-OPH microspheres did not show expected bio-sensing response in the fluorescence assay, which can be postulated to be because of interference of polymer in pH-based detection.

4. Discussion

In this study, we have demonstrated that His-Nus-OPH can show improved solubilization by including a NusA tag and yields enhanced

enzymatic activity for the degradation of organophosphate compounds. Incidentally, we observed that soluble protein was obtained when induction was performed at a lowered temperature of 16 °C compared to 37 °C. This is attributed to increased solubility of protein at lower temperatures owing to increased expression of chaperones in *E. coli* [56], reduced effect of heat shock proteases, and increased stability favouring proper folding patterns [57,58]. Additionally, growth at lower temperatures from 15 to 23 °C, brings a significant reduction in degradation of the expressed protein [59,60]. These factors allowed the proper solubilization of protein when induction was performed at 16 °C.

Alginate encapsulation has generally been used in a variety of applications in the literature, such as controlled drug release, oil encapsulation, nanoparticles, cells, and enzymes [61–68]. Many of these reports have focused on encapsulation with calcium alginate. In this report, we have successfully encapsulated FITC Dextran with or without His-Nus-OPH in sodium alginate beads, which poses an important advantage in terms of water solubility when compared to calcium alginate [69], resulting in decreased fluorescence quenching, higher fluorescence intensity when used with fluorescent dyes, and enhanced chemical availability for the encapsulated enzyme [70,71]. FITC has been known to be a versatile fluorophore with properties like pH sensitivity, the capability to conjugating polymer matrices, and ease of characterization by fluorometry and fluorescence microscopy. FITC-dextran (500 kDa) is also known to have similar fluorescence properties as FITC itself while having advantages in terms of water solubility, inert nature, non-toxicity, and reduced leachability from alginate matrices [72,73]. Co-immobilization of FITC-dextran with His-Nus-OPH has been shown in this report to aid in developing a fluorescent assay for the detection of OP compounds. The fluorescence of FITC-dextran is pH-dependent. Below pH 3, fluorescence intensity is minimum. At pH 4 and above, there is a linear increase in fluorescence intensity, which saturates at pH 8–9. In essence, acidic pH leads to loss of fluorescence intensity due to protonation of FITC, and basic pH leads to higher fluorescence intensity due to conversion into a mono-anionic or di-anionic form [53,74].

With respect to the colorimetric assay, an increase in the specific activity is observed with an increase in substrate concentration of ethyl paraoxon and methyl parathion due to the progressive access of substrate to the active sites of His-Nus-OPH. Consequently, the intensity of the yellow colour observed due to the production of *p*-nitrophenol also increases. Interestingly, it is observed that in the colorimetric tests, the sensitivity of the encapsulated His-Nus-OPH is lower than that of soluble His-Nus-OPH. Moreover, a higher response time was seen for the encapsulated His-Nus-OPH compared to the soluble enzyme. This may be due to the loss of some enzyme activity to the substrate after encapsulation [75]. Nevertheless, the encapsulated enzyme does exhibit improvements in terms of LOD while maintaining similar linearity as the solution-phase His-Nus-OPH.

Typically, using fluorescence techniques for the detection of OP compounds should provide a lower detection limit which can also be seen in the current study. Use of His-Nus-OPH enzyme in the fluorescence assay demonstrated a lower LOD of 0.014 mM and 0.044 mM for ethyl paraoxon and methyl parathion, respectively, which was found to be superior compared to the colorimetric biosensing. The linear range and response time in both colorimetric and fluorescent sensing both are comparable (5 min) which is mainly a function of enzyme activity of His-Nus-OPH. The results also clearly indicate that although both colorimetric and fluorometric methods can be used for estimation, however, owing to its sensitivity, FITC dextran-based estimation would be preferable for the development of biosensor assays and devices.

5. Conclusion

In this study, it is demonstrated that NusA-tagged OPH (His-Nus-OPH) was found to be soluble and hence purified to be used in colorimetric and fluorometric assays for organophosphate detection. We have demonstrated that His-Nus-OPH yields enhanced enzymatic activity for the degradation of organophosphate compounds while being a good candidate for use as a colorimetric biosensor when encapsulated with alginate microspheres. Our study indicates good specific activity for the purified His-Nus-OPH, i.e. 333 U/mg and 90.2 U/mg for ethyl paraoxon and methyl parathion, respectively. Solution phase His-Nus-OPH protein and protein encapsulated using a novel method of ultrasonic atomization was used in a colorimetric assay where encapsulated protein gave improved LOD than solution-phase His-Nus-OPH with a similar linear range of substrates. A fluorescence-based method was also established using FITC dextran for solution-phase His-Nus-OPH. Fluorescence emission drop suggested a linear decrease over a concentration range of 0.001–0.5 mM in the case of ethyl paraoxon, and 0.005–0.5 mM in the case of methyl parathion, respectively. As expected, the limit of detection was found to superior for fluorescence assay than a colorimetric assay for ethyl paraoxon and methyl parathion. The results indicate that the NusA-tagged OPH enzyme can be used in both colorimetric and fluorescence-based sensor systems with good detection limits, response time, and linearity. Future research efforts to further enhance the performance should be focused on structural modifications to enhance the catalytic activity, as well as enhancing the long-term stability of the sensor.

Declaration of competing interest

The authors declare no competing interests.

Acknowledgements

We are grateful to Prof. D. Siddavattam (Dept. of Animal Biology, School of Life Sciences, University of Hyderabad, Hyderabad-500046, India) for providing the *opd* gene for the study. A.J. would like to thank SERB-ECR and DST-INSPIRE faculty award. In addition, M.J. and B.J. are thankful to the Ministry of Human Resource Development (MHRD), Government of India, and Department of Science and Technology (DST), Government of India, for PhD fellowship.

Appendix A. Supplementary data

Supplementary data to this article can be found online at https://doi.org/10.1016/j.pep.2021.105929.

Authors contributions

P. Kodgire, A. Joshi, and M. Jain designed the experiments; M. Jain performed the experiments, analysed the data; P. Yadav and B. Joshi coordinated some of the experiments; M. Jain wrote the draft of the manuscript and P. Kodgire and A. Joshi edited and revised the manuscript.

Funding

No competing financial interests have been declared. Funding for this work was provided by the Department of Biotechnology, Govt. of India, for a research grant (BT/PR20319/BBE/117/189/2016 and BT/PR24652/NER/95/795/2017).

Ethical approval

This article does not contain any studies with human participants or animals performed by any of the authors.

References

[1] V. Silva, H.G.J. Mol, P. Zomer, M. Tienstra, C.J. Ritsema, V. Geissen, Pesticide residues in European agricultural soils – a hidden reality unfolded, Sci. Total

Environ. 653 (2019) 1532–1545, https://doi.org/10.1016/j.scitotenv.2018.10.441.
[2] S. Karami-Mohajeri, M. Abdollahi, Toxic influence of organophosphate, carbamate, and organochlorine pesticides on cellular metabolism of lipids, proteins, and carbohydrates: a systematic review, Hum. Exp. Toxicol. 30 (2011) 1119–1140, https://doi.org/10.1177/0960327110388959.
[3] E.E.K. Clarke, L.S. Levy, A. Spurgeon, I.A. Calvert, The problems associated with pesticide use by irrigation workers in Ghana, Occup. Med. (Phila.) 47 (1997) 301–308, https://doi.org/10.1093/occmed/47.5.301.
[4] D. Atwood, C. Paisley-Jones, US EPA - Pesticides Industry Sales and Usage 2008 - 2012, 2008.
[5] F.M. Dyro, Organophosphates, neurol. https://emedicine.medscape.com/article/1175139-overview, 2016.
[6] M. Eddleston, L. Karalliedde, N. Buckley, R. Fernando, G. Hutchinson, G. Isbister, F. Konradsen, D. Murray, J.C. Piola, N. Senanayake, R. Sheriff, S. Singh, S. B. Siwach, L. Smit, Pesticide poisoning in the developing world - a minimum pesticides list, Lancet 360 (2002) 1163–1167, https://doi.org/10.1016/S0140-6736(02)11204-9.
[7] J.B. Ortiz-Delgado, V. Funes, C. Sarasquete, The organophosphate pesticide -OP-malathion inducing thyroidal disruptions and failures in the metamorphosis of the Senegalese sole, Solea senegalensis, BMC Vet. Res. 15 (2019) 3–21, https://doi.org/10.1186/s12917-019-1786-z.
[8] J. Yang, C. Yang, H. Jiang, C. Qiao, Overexpression of methyl parathion hydrolase and its application in detoxification of organophosphates, Biodegradation 19 (2008) 831–839, https://doi.org/10.1007/s10532-008-9186-2.
[9] F.L. Watson, H. Schmidt, Z.K. Turman, N. Hole, H. Garcia, J. Gregg, J. Tilghman, E. A. Fradinger, Organophosphate pesticides induce morphological abnormalities and decrease locomotor activity and heart rate in Danio rerio and Xenopus laevis, Environ. Toxicol. Chem. 33 (2014) 1337–1345, https://doi.org/10.1002/etc.2559.
[10] J. Bajgar, J. Fusek, K. Kuca, L. Bartosova, D. Jun, Treatment of organophosphate intoxication using cholinesterase reactivators:facts and fiction, Mini Rev. Med. Chem. 7 (2007) 461–466, https://doi.org/10.2174/138955707780619581.
[11] D.B. Headley, Effects of atropine sulfate and pralidoxime chloride on visual, physiological, performance, subjective, and cognitive variables in man: a review, Mil. Med. 147 (1982) 122–133, https://doi.org/10.1093/milmed/147.2.122.
[12] R. Rahimi, S. Nikfar, M. Abdollahi, Increased morbidity and mortality in acute human organophosphate-poisoned patients treated by oximes: a meta-analysis of clinical trials, Hum. Exp. Toxicol. 25 (2006) 157–162, https://doi.org/10.1191/0960327106ht602oa.
[13] M. Jokanović, M. Kosanović, D. Brkić, P. Vukomanović, Organophosphate induced delayed polyneuropathy in man: an overview, Clin. Neurol. Neurosurg. 113 (2011) 7–10, https://doi.org/10.1016/j.clineuro.2010.08.015.
[14] H. Sungurtekin, E. Gürses, C. Balci, Evaluation of several clinical scoring tools in organophosphate poisoned patients, Clin. Toxicol. 44 (2006) 121–126, https://doi.org/10.1080/15563650500514350.
[15] U.A.D.D. Munidasa, I.B. Gawarammana, S.A.M. Kularatne, P.V.R. Kumarasiri, C.D. A. Goonasekera, Survival pattern in patients with acute organophosphate poisoning receiving intensive care, J. Toxicol. Clin. Toxicol. 42 (2004) 343–347, https://doi.org/10.1081/CLT-120039539.
[16] M. Sungur, M. Güven, Intensive care management of organophosphate insecticide poisoning, Crit. Care 5 (2001) 211–215, https://doi.org/10.1186/cc1025.
[17] H. Hrabetz, H. Thiermann, N. Felgenhauer, T. Zilker, B. Haller, J. Nähring, B. Saugel, F. Eyer, Organophosphate poisoning in the developed world – a single centre experience from here to the millennium, Chem. Biol. Interact. 206 (2013) 561–568, https://doi.org/10.1016/j.cbi.2013.05.003.
[18] J. Laveglia, P.A. Dahm, Degradation of organophosphorus and carbamate insecticides in the soil and by soil microorganisms, Annu. Rev. Entomol. 22 (1977) 483–513, https://doi.org/10.1146/annurev.en.22.010177.002411.
[19] D.G. Kang, L. Li, J.H. Ha, S.S. Choi, H.J. Cha, Efficient cell surface display of organophosphorous hydrolase using N-terminal domain of ice nucleation protein in Escherichia coli, Kor. J. Chem. Eng. 25 (2008) 804–807, https://doi.org/10.1007/s11814-008-0132-0.
[20] M. Shimazu, W. Chen, A. Mulchandani, Biological detoxification of organophosphate pesticides, ACS Symp. Ser. 863 (2003) 25–36, https://doi.org/10.1021/bk-2004-0863.ch003.
[21] E. Ghanem, F.M. Raushel, Detoxification of organophosphate nerve agents by bacterial phosphotriesterase, Toxicol. Appl. Pharmacol. 207 (2005) 459–470, https://doi.org/10.1016/j.taap.2005.02.025.
[22] F.M. Raushel, Bacterial detoxification of organophosphate nerve agents, Curr. Opin. Microbiol. 5 (2002) 288–295, https://doi.org/10.1016/S1369-5274(02)00314-4.
[23] E. Carletti, L. Jacquamet, M. Loiodice, D. Rochu, P. Masson, F. Nachon, Update on biochemical properties of recombinant Pseudomonas diminuta phosphotriesterase, J. Enzym. Inhib. Med. Chem. 24 (2009) 1045–1055, https://doi.org/10.1080/14756360802608518.
[24] C.J. Jackson, J.L. Foo, H.K. Kim, P.D. Carr, J.W. Liu, G. Salem, D.L. Ollis, In crystallo capture of a michaelis complex and product-binding modes of a bacterial phosphotriesterase, J. Mol. Biol. 375 (2008) 1189–1196, https://doi.org/10.1016/j.jmb.2007.10.061.
[25] C.M.H. Cho, A. Mulchandani, W. Chen, C. Mee-Hie Cho, A. Mulchandani, W. Chen, Functional analysis of organophosphorus hydrolase variants with high degradation activity towards organophosphate pesticides, Protein Eng. Des. Sel. 19 (2006) 99–105, https://doi.org/10.1093/protein/gzj007.
[26] M. Jain, P. Yadav, A. Joshi, P. Kodgire, Advances in detection of hazardous organophosphorus compounds using organophosphorus hydrolase based biosensors, Crit. Rev. Toxicol. 49 (2019), https://doi.org/10.1080/10408444.2019.1626800.
[27] A.N. Bigley, F.M. Raushel, The evolution of phosphotriesterase for decontamination and detoxification of organophosphorus chemical warfare agents, Chem. Biol. Interact. 308 (2019) 80–88, https://doi.org/10.1016/j.cbi.2019.05.023.
[28] S. Xiong, Y. Deng, Y. Zhou, D. Gong, Y. Xu, L. Yang, H. Chen, L. Chen, T. Song, A. Luo, X. Deng, C. Zhang, Z. Jiang, Current progress in biosensors for organophosphorus pesticides based on enzyme functionalized nanostructures: a review, Anal. Methods. 10 (2018) 5468–5479, https://doi.org/10.1039/c8ay01851k.
[29] M.M. Meier, C. Rajendran, C. Malisi, N.G. Fox, C. Xu, S. Schlee, D.P. Barondeau, B. Höcker, R. Sterner, F.M. Raushel, Molecular engineering of organophosphate hydrolysis activity from a weak promiscuous lactonase template, J. Am. Chem. Soc. 135 (2013) 11670–11677, https://doi.org/10.1021/ja405911h.
[30] P.K. Robinson, Enzymes: principles and biotechnological applications, Essays Biochem. 59 (2015) 1–41, https://doi.org/10.1042/BSE0590001.
[31] G. Pandey, S. Choudhary, R. Chaudhari, A. Joshi, Ultrasonic atomizer based development of pH sensor for real time analysis, Sci. Rep. 10 (2020) 10910, https://doi.org/10.1038/s41598-020-68005-2.
[32] R. Dhirhi, K. Prasad, A.K. Shukla, S. Sarkar, T. Renganathan, S. Pushpavanam, M. Kaza, Experimental study of rotating dry slag granulation unit: operating regimes, particle size analysis and scale up, Appl. Therm. Eng. 107 (2016) 898–906, https://doi.org/10.1016/j.applthermaleng.2016.07.049.
[33] M. Zourob, A. Simonian, J. Wild, S. Mohr, X. Fan, I. Abdulhalim, N.J. Goddard, Optical leaky waveguide biosensors for the detection of organophosphorus pesticides, Analyst 132 (2007) 114–120, https://doi.org/10.1039/b612871h.
[34] R.A. Doong, H.C. Tsai, Immobilization and characterization of sol-gel-encapsulated acetylcholinesterase fiber-optic biosensor, Anal. Chim. Acta 434 (2001) 239–246, https://doi.org/10.1016/S0003-2670(01)00853-4.
[35] X. Cao, S.V. Mello, R.M. Leblanc, V.K. Rastogi, T.C. Cheng, J.J. DeFrank, Detection of paraoxon by immobilized organophosphorus hydrolase in a Langmuir-Blodgett film, Colloids Surfaces A Physicochem. Eng. Asp. 250 (2004) 349–356, https://doi.org/10.1016/j.colsurfa.2004.01.043.
[36] J.M. Itkonen, A. Urtti, L.E. Bird, S. Sarkhel, Codon optimization and factorial screening for enhanced soluble expression of human ciliary neurotrophic factor in Escherichia coli, BMC Biotechnol. 14 (2014) 92, https://doi.org/10.1186/s12896-014-0092-x.
[37] N. Habibi, S.Z. Mohd Hashim, A. Norouzi, M.R. Samian, A review of machine learning methods to predict the solubility of overexpressed recombinant proteins in Escherichia coli, BMC Bioinf. 15 (2014) 134, https://doi.org/10.1186/1471-2105-15-134.
[38] M.R. Bell, M.J. Engleka, A. Malik, J.E. Strickler, To fuse or not to fuse: what is your purpose? Protein Sci. 22 (2013) 1466–1477, https://doi.org/10.1002/pro.2356.
[39] A. Spriestersbach, J. Kubicek, F. Schäfer, H. Block, B. Maertens, Purification of his-tagged proteins, Methods Enzymol. 559 (2015) 1–15, https://doi.org/10.1016/bs.mie.2014.11.003.
[40] S. Nallamsetty, D.S. Waugh, Solubility-enhancing proteins MBP and NusA play a passive role in the folding of their fusion partners, Protein Expr, Purif 45 (2006) 175–182, https://doi.org/10.1016/j.pep.2005.06.012.
[41] X.Y. Liu, F.F. Chen, C.X. Li, X.J. Luo, Q. Chen, Y.P. Bai, J.H. Xu, Improved efficiency of a novel methyl parathion hydrolase using consensus approach, Enzym. Microb. Technol. 93–94 (2016) 11–17, https://doi.org/10.1016/j.enzmictec.2016.07.005.
[42] Q.-Y. Dong, M.-Y. Chen, Y. Xin, X.-Y. Qin, Z. Cheng, L.-E. Shi, Z.-X. Tang, Alginate-based and protein-based materials for probiotics encapsulation: a review, Int. J. Food Sci. Technol. 48 (2013) 1339–1351, https://doi.org/10.1111/ijfs.12078.
[43] S.A. Chaudhari, J.R. Kar, R.S. Singhal, Immobilization of proteins in alginate: functional properties and applications, Curr. Org. Chem. 19 (2015) 1732–1754, https://doi.org/10.2174/1385272819666150429232110.
[44] J.Y. Leong, W.H. Lam, K.W. Ho, W.P. Voo, M.F.X. Lee, H.P. Lim, S.L. Lim, B.T. Tey, D. Poncelet, E.S. Chan, Advances in fabricating spherical alginate hydrogels with controlled particle designs by ionotropic gelation as encapsulation systems, Particuology 24 (2016) 44–60, https://doi.org/10.1016/j.partic.2015.09.004.
[45] A. Joshi, R. Keerthiprasad, R.D. Jayant, R. Srivastava, Nano-in-micro alginate based hybrid particles, Carbohydr. Polym. 81 (2010) 790–798, https://doi.org/10.1016/j.carbpol.2010.03.050.
[46] E.S. Kim, J.-S. Lee, H.G. Lee, Calcium-alginate microparticles for sustained release of catechin prepared via an emulsion gelation technique, Food Sci. Biotechnol. 25 (2016) 1337–1343, https://doi.org/10.1007/s10068-016-0210-8.
[47] H. Jiang, R. Tian, W. Hu, Y. Jia, P. Yuan, J. Wang, L. Zhang, Formulation and evaluation of gastroretentive floating drug delivery system of dipyridamole, Drug Dev. Ind. Pharm. 41 (2015) 674–680, https://doi.org/10.3109/03639045.2014.893355.
[48] H. Park, P.H. Kim, T. Hwang, O.J. Kwon, T.J. Park, S.W. Choi, C.O. Yun, J.H. Kim, Fabrication of cross-linked alginate beads using electrospraying for adenovirus delivery, Int. J. Pharm. 427 (2012) 417–425, https://doi.org/10.1016/j.ijpharm.2012.01.050.
[49] O. Sandoval-Castilla, C. Lobato-Calleros, H.S. García-Galindo, J. Alvarez-Ramírez, E.J. Vernon-Carter, Textural properties of alginate-pectin beads and survivability of entrapped Lb. casei in simulated gastrointestinal conditions and in yoghurt, Food Res. Int. 43 (2010) 111–117, https://doi.org/10.1016/j.foodres.2009.09.010.
[50] C.M.-H.H. Cho, A. Mulchandani, W. Chen, Bacterial cell surface display of organophosphorus hydrolase for selective screening of improved hydrolysis of

organophosphate nerve agents, Appl. Environ. Microbiol. 68 (2002) 2026–2030, https://doi.org/10.1128/AEM.68.4.2026-2030.2002.
[51] Y. Chen, C. Zhu, J. Cen, Y. Bai, W. He, Z. Guo, Ratiometric detection of pH fluctuation in mitochondria with a new fluorescein/cyanine hybrid sensor, Chem. Sci. 6 (2015) 3187–3194, https://doi.org/10.1039/c4sc04021j.
[52] B. Prieto-Simón, M. Campàs, S. Andreescu, J.L. Marty, Trends in flow-based biosensing systems for pesticide assessment, Sensors 6 (2006) 1161–1186, https://doi.org/10.3390/s6101161.
[53] R. Chaudhari, A. Joshi, R. Srivastava, PH and urea estimation in urine samples using single fluorophore and ratiometric fluorescent biosensors, Sci. Rep. 7 (2017) 5840, https://doi.org/10.1038/s41598-017-06060-y.
[54] C. Wischke, H.H. Borchert, Fluorescein isothiocyanate labelled bovine serum albumin (FITC-BSA) as a model protein drug: opportunities and drawbacks, Pharmazie 61 (2006) 770–774.
[55] G. Gauglitz, Analytical evaluation of sensor measurements, Anal. Bioanal. Chem. 410 (2018) 5–13, https://doi.org/10.1007/s00216-017-0624-z.
[56] M. Ferrer, T.N. Chernikova, M.M. Yakimov, P.N. Golyshin, K.N. Timmis, Chaperonins govern growth of Escherichia coli at low temperatures, Nat. Biotechnol. 21 (2003) 1266–1267, https://doi.org/10.1038/nbt1103-1266.
[57] A. Vera, N. González-Montalbán, A. Arís, A. Villaverde, The conformational quality of insoluble recombinant proteins is enhanced at low growth temperatures, Biotechnol. Bioeng. 96 (2007) 1101–1106, https://doi.org/10.1002/bit.21218.
[58] S. Sahdev, S.K. Khattar, K.S. Saini, Production of active eukaryotic proteins through bacterial expression systems: a review of the existing biotechnology strategies, Mol. Cell. Biochem. 307 (2008) 249–264, https://doi.org/10.1007/s11010-007-9603-6.
[59] C. Spiess, A. Beil, M. Ehrmann, A temperature-dependent switch from chaperone to protease in a widely conserved heat shock protein, Cell 97 (1999) 339–347, https://doi.org/10.1016/S0092-8674(00)80743-6.
[60] S. Hunke, J.-M. Betton, Temperature effect on inclusion body formation and stress response in the periplasm of Escherichia coli, Mol. Microbiol. 50 (2003) 1579–1589, https://doi.org/10.1046/j.1365-2958.2003.03785.x.
[61] B.B. Mandal, S.C. Kundu, Calcium alginate beads embedded in silk fibroin as 3D dual drug releasing scaffolds, Biomaterials 30 (2009) 5170–5177, https://doi.org/10.1016/j.biomaterials.2009.05.072.
[62] S.K. Yadav, G. Khan, G.V. Bonde, M. Bansal, B. Mishra, Design, optimization and characterizations of chitosan fortified calcium alginate microspheres for the controlled delivery of dual drugs, Artif. Cells, Nanomedicine, Biotechnol. 46 (2018) 1180–1193, https://doi.org/10.1080/21691401.2017.1366331.
[63] C.H. Yeh, Q. Zhao, S.J. Lee, Y.C. Lin, Using a T-junction microfluidic chip for monodisperse calcium alginate microparticles and encapsulation of nanoparticles, Sensors Actuators, A Phys. 151 (2009) 231–236, https://doi.org/10.1016/j.sna.2009.02.036.
[64] R. Stojanovic, A. Belscak-Cvitanovic, V. Manojlovic, D. Komes, V. Nedovic, B. Bugarski, Encapsulation of thyme (Thymus serpyllum L.) aqueous extract in calcium alginate beads, J. Sci. Food Agric. 92 (2012) 685–696, https://doi.org/10.1002/jsfa.4632.
[65] T. Haider, Q. Husain, Hydrolysis of milk/whey lactose by β galactosidase: a comparative study of stirred batch process and packed bed reactor prepared with calcium alginate entrapped enzyme, Chem. Eng. Process. Process Intensif. 48 (2009) 576–580, https://doi.org/10.1016/j.cep.2008.02.007.
[66] E.S. Chan, S.L. Wong, P.P. Lee, J.S. Lee, T.B. Ti, Z. Zhang, D. Poncelet, P. Ravindra, S.H. Phan, Z.H. Yim, Effects of starch filler on the physical properties of lyophilized calcium-alginate beads and the viability of encapsulated cells, Carbohydr. Polym. 83 (2011) 225–232, https://doi.org/10.1016/j.carbpol.2010.07.044.
[67] J.C. Duarte, J.A.R. Rodrigues, P.J.S. Moran, G.P. Valença, J.R. Nunhez, Effect of immobilized cells in calcium alginate beads in alcoholic fermentation, Amb. Express 3 (2013) 1–8, https://doi.org/10.1186/2191-0855-3-31.
[68] P.W. Ren, X.J. Ju, R. Xie, L.Y. Chu, Monodisperse alginate microcapsules with oil core generated from a microfluidic device, J. Colloid Interface Sci. 343 (2010) 392–395, https://doi.org/10.1016/j.jcis.2009.11.007.
[69] A. Shilpa, S.S. Agrawal, A.R. Ray, Controlled delivery of drugs from alginate matrix, J. Macromol. Sci. Polym. Rev. 43 (2003) 187–221, https://doi.org/10.1081/MC-120020160.
[70] A.L. Koner, W.M. Nau, Cucurbituril encapsulation of fluorescent dyes, Supramol. Chem. 19 (2007) 55–66, https://doi.org/10.1080/10610270600910749.
[71] N. Realdon, E. Ragazzi, E. Ragazzi, Effect of drug solubility on in vitro availability rate from suppositories with polyethylene glycol excipients, Pharmazie 56 (2001) 163–167. https://europepmc.org/article/med/11234347 (accessed June 7, 2020).
[72] E. Lanz, M. Gregor, J. Slavík, A. Kotyk, Use of FITC as a fluorescent probe for intracellular pH measurement, J. Fluoresc. 7 (1997) 317–319, https://doi.org/10.1023/A:1022586127784.
[73] F.J. Alvarez, A. Herráez, M.C. Tejedor, Fluorescence analysis of carrier rat and human erythrocytes loaded with FITC-Dextran, Cytometry 24 (1996) 181–189, https://doi.org/10.1002/(SICI)1097-0320(19960601)24:2<181::AID-CYTO11>3.0.CO;2-N.
[74] R.D. Chaudhari, A.B. Joshi, K. Pandya, R. Srivastava, pH based urea biosensing using fluorescein isothiocyanate (FITC)-dextran encapsulated micro-carriers of calcium alginate, Sens. Lett. 14 (2016) 451–459, https://doi.org/10.1166/sl.2016.3663.
[75] Y.V. Plekhanova, S.A. Tikhonenko, A.V. Dubrovsky, A.L. Kim, E.V. Musin, G. J. Wang, I.E. Kuznetsova, V.V. Kolesov, A.N. Reshetilov, Comparative study of electrochemical sensors based on enzyme immobilized into polyelectrolyte microcapsules and into chitosan gel, Anal. Sci. 35 (2019) 1037–1043, https://doi.org/10.2116/analsci.19P131.